SCANNING VOL. 32, 294–303 (2010)


# Evolution of ZDDP-Derived Reaction Layer Morphology With Rubbing Time

A. NAVEIRA-SUAREZ[1,2], A. TOMALA[3], R. PASARIBU[1], R. LARSSON[2], AND I. C. GEBESHUBER[3,4,5]

[1]SKF Engineering and Research Centre, Nieuwegein, The Netherlands
[2]Division of Machine Elements, Luleå University of Technology, Luleå, Sweden
[3]Institute of Applied Physics, Vienna University of Technology, Wien, Austria
[4]Institute of Microengineering and Nanoelectronics, Universiti Kebangsaan Malaysia, Bangi, Malaysia
[5]AC2T Austrian Center of Competence for Tribology, Wiener Neustadt, Austria

**Summary:** Functional additives, particularly extreme pressure and antiwear additives, in formulated oil will compete to adsorb and function in tribological contacts. A low-polarity commercial base oil, poly-α-olefin (PAO), blended with zinc dialkyl dithiophosphates (ZDDP) has been studied. The tribological performance was evaluated using a ball-on-disk test rig under mixed rolling–sliding conditions in the boundary lubrication regime at 90°C. An adapted *in situ* interferometry technique was used to monitor the additive-derived reaction layer formation. The thickness of the reaction layer evolves with rubbing until reaching a limiting thickness value of approximately 70 nm. The evolution of the topography and mechanical properties of the ZDDP-derived reaction layer with rubbing time were studied using Atomic Force Microscopy. A constant roughening and hardening of the additive-derived layer with rubbing time is observed and related to the different tribological performance of the layer at different rubbing times. SCANNING 32: 294–303, 2010. © 2010 Wiley Periodicals, Inc.

**Key words:** additives, AFM, atomic force microscopy, boundary layers formation, boundary lubrication, morphology, nanowear, reaction layer, ZDDP

Address for reprints: I. C. Gebeshuber, Institute of Microengineering and Nanoelectronics (IMEN), Universiti Kebangsaan Malaysia, 43600 UKM, Bangi, Selangor, Malaysia
E-mail: ille.gebeshuber@mac.com

Received 3 August 2010; Accepted with revision 21 September 2010

DOI 10.1002/sca.20207
Published online 22 October 2010 in Wiley Online Library (wileyonlinelibrary.com)

## Introduction

Extreme pressure (EP) and antiwear additives (AW) control the performance of lubricants in the mixed and boundary lubrication regimes. Performance-enhancing properties of these additives are very important as, if oil lacks lubricating ability, excessive wear and friction can occur (American Society for Metals 1992). The main elements, which are responsible for the EP and AW action, are sulfur and phosphorus, respectively (Sakamoto *et al.* 1985).

Metal dialkyl dithiophosphate compounds have been used in lubricating oils due to their multifunctional performance as AW, EP, friction modifying, antioxidant and corrosion inhibiting additives. Dialkyl dithiophosphates of different metals, such as molybdenum (Sarin *et al.* 1994), cadmium (Jianqiang *et al.* 2005), copper (Zhang *et al.* 1998), titanium, gadolinium (Boshui *et al.* 1996), iron, antimony, and other metals, have been introduced in lubricants, albeit zinc dialkyl dithiophosphates (ZDDP) are the most widely used (Barnes *et al.* 2001; Georges *et al.* 1979; Watkins and Spedding 1982; Spedding and Watkins 1982; Gellman and Spencer 2002).

ZDDP reacts with the surface in contact to form protective reaction layers. A variety of mechanisms have been proposed (Bancroft *et al.* 1997) for the formation of the ZDDP-derived reaction layers, involving oxidative (by reaction with hydroperoxides or peroxy radicals) (Willermet *et al.* 1995a), catalytic (chemisorption on metal, hydrolytic, Spedding and Watkins 1982), and thermal (Coy and Jones 1981) decomposition of the ZDDP. The additive decomposes under certain conditions and the decomposition products react to generate a 50–150 nm thick layer (Bec *et al.* 1999; Fujita and Spikes 2004; Minfray *et al.* 2004). The resulting

reaction layers have a heterogeneous composition with the chemical structure of the starting materials dictating their chemical composition (Fuller *et al.* 1997; Yin *et al.* 1993). The structure and chemical composition of the layer have been analyzed using advanced spectroscopy techniques, such as X-ray photoelectron spectroscopy (Bird and Galvin 1976; Eglin *et al.* 2003; Piras *et al.* 2003; Heuberger *et al.* 2007a,b), Auger electron spectroscopy (Minfray *et al.* 2006), and X-ray absorption near edge spectroscopy (Fuller *et al.* 1997; Yin *et al.* 1997), and found to be dependent on temperature and tribological conditions. The layers are composed of a mixture of short and long polyphosphates (Bancroft *et al.* 1997; Willermet *et al.* 1997) with the presence of sulfides and oxides in the layer bulk (Willermet *et al.* 1995b). A two-layer structure for the ZDDP-derived reaction layers has also been proposed, where a thin long chain zinc poly(thio)-phosphate layer is superimposed on a thicker short chain mixed Fe/Zn polyphosphate layer, containing embedded nanocrystallites of ZnO and ZnS (Martin *et al.* 2001).

However, several studies have proven ZDDP to have detrimental effects on wear under certain operation conditions (Torrance *et al.* 1996) and to enhance friction when the system is operating in mixed and boundary lubrication regimes (Taylor *et al.* 2000; Taylor and Spikes 2003).

Atomic Force Microscopy (AFM) allows the study of surfaces at the nanoscale, providing a method of measuring ultra small forces between a single asperity probe tip and the surface of the sample. Therefore, it is a suitable instrument to study engineering surfaces under dry or wet conditions with atomic resolution. Thus, the atomic-scale origins of friction could be observed with this technique. Transition from single (nanoscale) asperity to multiple asperity contacts holds the promise to predict tribological behavior. AFM was previously used to address the nanoscale origins of the effect of base oil polarity on friction and wear behavior of ZDDP-derived reaction layers (Tomala *et al.* 2009) using low-viscosity model base oils. Force vs. distance plots are often used to measure the interaction forces between the tip and the surface, by pushing the tip against the surface, and then separating the tip and surface. From this data adhesion, indentation and layer elasticity can be studied. It was found that base oil polarity determines the transport of additives to the surface thereby controlling the maximum reaction layer thickness, friction and wear, as well as the morphology of the additive-derived reaction layer. However, the reaction layer chemical composition is not strongly influenced by the base oil polarity (Naveira-Suarez *et al.* 2009). The same behavior was observed when using ZDDP in solution with commercial base oils of different polarities and among the operating conditions, shear was identified as a fundamental parameter on the activation of additives on rubbing steel surfaces and the properties of the derived reaction layer (Naveira-Suarez *et al.* 2010). In this article, we study the evolution of the reaction layer with rubbing time and its nanofriction and nanowear behavior, to further understand the differences observed in the friction and wear performance.

## Materials and Methods

### Test Samples

The Ø20-mm steel balls were AISI 52100 steel with hardness 59–66 HRC and an average roughness (Ra) of 10 nm. The rings were washers (WS 81212) from SKF Cylindrical Thrust Roller Bearings of ASI 52100 steel with hardness 59–66 HRC and Ra = 100 nm. The specimens were cleaned before testing by successive immersion first in an ultrasonic bath of petroleum ether for 10 min and then acetone for 10 min.

### Lubricant

The lubricant selected as the base oil was poly-α-olefin (PAO), a synthetic non-polar oil. PAO was chosen over mineral oil because of its purity, as mineral oil has a relatively high concentration of sulfur, which might interfere with the additives. The physical properties, sulfur and phosphorus content, obtained by X-ray fluorescence analysis of the base oil samples before testing, are summarized in Table I.

It is assumed that the addition of the additives does not significantly change the viscosity of the bulk solution.

TABLE I Base oil properties

| Code | Kinematic viscosity at 40°C ($mm^2/s$) | Kinematic viscosity at 100°C ($mm^2/s$) | Sulfur content (wt%) | Phosphorus content (wt%) |
|---|---|---|---|---|
| PAO | 24.6 | 5.1 | 0.00055 | <0.00030 |

PAO, poly-α-olefin.

A fully formulated iso-$C_4$-zinc dialkyl dithiophosphate (ZDDP), with 99% purity is employed in simple solution in both base oils without other additives present. 2 wt% ZDDP solutions were prepared using an ultrasonic bath to dissolve the additives in the base oils. The temperature of the lubricant solution remained below 40°C during the dissolving procedure.

### Macro-Tribological Tests

SKF-WAM5 ball-on-disk test rig (Wedeven Associates, Inc., Edgmont, PA) enables the performance of a variety of tests to evaluate the tribological performance of additive/base oil blends under controlled contact conditions. The ball and the disk are independently driven, giving the possibility to simulate pure rolling and various slide-roll ratios (SRR). The SRR, or slip ratio, is defined as the sliding speed $U_S = U_B - U_R$ divided by the entrainment speed, or rolling speed, $U = (U_B + U_R)/2$, where $U_B$ and $U_R$ are the ball and ring surface speed in contact, respectively.

The effect of rubbing time in the morphology and properties of the ZDDP-derived reaction layer is studied in a mixed rolling/sliding contact, with wear evenly distributed in the tracks of both specimens. The tribotests were carried out at an applied load of 300 N, which resulted in a maximum Hertzian contact pressure of 1.9 GPa (contact diameter 540 μm) at a SRR = −10%. The temperature was set constant at 90°C for all the tests. The specific film thickness or lambda ratio (the ratio of the central film thickness to the composite surface roughness of the two surfaces is contact) was set constant at 0.4 and the entrainment speed was set accordingly to 0.25 m/s. The system was operating in the boundary lubrication regime.

### Spacer Layer Interferometry

Spacer layer interferometry imaging principle (Cann *et al.* 1996) is used as an *in situ* (inside the tribometer, out of the contact) and *post mortem* (after friction) method (Donnet 1998) to monitor reaction layer formation (Fujita and Spikes 2004). Tests are carried out by rolling/sliding a steel ball on a lubricated steel disk, to produce a wear track on both ball and disk. Motion is halted and a spacer layer and chromium-coated glass disk are loaded against the wear track on the steel ball. The lubricant is squeezed out from the contact, but any solid-like reaction layer remains. A contact is formed between the reflective steel ball and the flat surface of a glass disk, which is coated with a thin chromium layer and a thicker silica spacer layer. White light is shown through the glass disk into the contact, where some of the light is reflected from the semi-reflecting chromium layer while the rest passes through the spacer layer and any transparent reaction layer present. Because the two beams have travelled different distances, they interfere constructively and destructively at wavelengths dependent on the path difference, to produce a colored interference image (Cann *et al.* 1996). The interference image produced is frame-grabbed and the color of each pixel is analyzed to determine the corresponding path difference and thus layer thickness, based on a calibration procedure. The interference images are a map of the reaction layer present in the contact. Once the image of the reaction layer formed at the rubbing steel ball is taken, the glass disk is then removed and the sliding/rolling of the steel ball on the steel disk continues.

### Nanotribological Tests: AFM

AFM and Lateral Force Microscopy (LFM) images of the wear track after the tribotests were obtained with an AFM MFP-3D (Asylum Research, Santa Barbara, CA) in ambient conditions. Silicon nitride tips (supplied by Veeco) on a V-shaped triangular cantilever with a low spring constant were used for nanotribological tests (friction measurements). Silicon tips on an aluminium-coated cantilever (OLYMPUS OMCL-HA) were used to perform nanowear tests. The important features of both cantilever types used for the study are listed in Table II. The cantilevers were calibrated for topography mode and pull-off force mode using a silicon chip. The value of spring constant for silicon nitride tips was 0.1 N/m, and for silicon tips

TABLE II Major features of the cantilever used for the AFM study

| | Cantilever V type VEECO (Topography and LFM) | Cantilever OLYMPUS OMCL-HA (Scratching, nanowear test) |
|---|---|---|
| Material | $Si_3N_4$ | Si coated with Al |
| Cantilever spring constant | 0.1 N/m | 42 N/m |
| Cantilever arm length, width | 140 μm, 18 μm | 160 μm, 50 μm |
| Resonance frequency | 38 kHz | 300 kHz |
| Full tip opening angle | 35° | – |
| Tip radius | 10 nm | < 10 nm |

was 42 N/m. The scan area was $5 \times 5\ \mu m^2$. Images were recorded in the contact mode, i.e. the feedback electronics and the corresponding software was used to keep the cantilever at constant deflection measuring the sample topography. In order to obtain the maximum LFM signal (torsion motion), the sample was scanned along the direction perpendicular to the cantilever long axis. The lateral force was evaluated from the difference in the torsional signals (displayed as output voltage) at forward and reverse scans on the lateral force (friction) loop. For each applied force, 512 lateral force loops on an area of $5\ \mu m^2$ were obtained from different regions. For wear measurement, all samples were scratched 40 times using a silicon tip on an aluminium-coated cantilever with a very high spring constant (42 N/m). The load applied to cantilever was 22 μN (equal to set point of 8 V), the scratching speed was 25 μm/s, scanning direction was perpendicular to the cantilever long axis and perpendicular to the wear track direction. After the scratching, topography of the scratched area was measured. The extent of wear was estimated by determining the average depth and width of the scratched area.

## Results and Discussion

### Macrotribological Tests

A series of interference images of the centre of the wear track derived from the PAO+ZDDP solution (low-polarity base oil) from the rubbing times are shown in Figure 1. In all the images, the sliding direction is from bottom to top. It can be seen that a reaction layer, evidently from the color scale in the images, develops differently due to the increase on rubbing time.

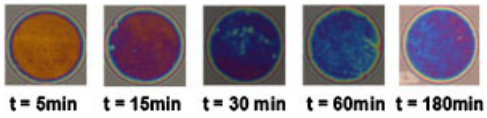


Fig 1. Series of interference images from different positions of the wear track for PAO+ZDDP at rubbing times $t = 5$, 15, 30, 60, and 180 min. ZDDP, zinc dialkyl dithiophosphates; PAO, poly-α-olefin.

From the interference images, reaction layer thickness values were determined at each position across a horizontal profile of the contact. From those values, the mean reaction layer thickness at the centre of the contact was calculated. The AW properties and average friction coefficient of the reaction layers derived from PAO+ZDDP solutions at different rubbing times were also investigated. The wear track width (WTW) was measured from the balls using a calibrated optical microscope. The friction coefficient is continuously recorded during the tribological tests and from these data the average friction coefficient is calculated. The results are summarized in Table III.

The evolution of the ZDDP-derived reaction layer thickness shows how initially a thick layer quickly develops with rubbing time, before stabilizing at a "limiting thickness." It is possible to identify an initial activation stage when the additive molecules are activated by the tribological energy and approach the surface. The growth mechanism begins with distinct reaction events on microasperity contact at the steel surfaces, leading to distinct segregated pads. The reaction layer develops initially very rapidly with the rate of formation being higher than the rate of removal. This suggests that the layer formation may be strongly catalysed by chemical species generated or released during rubbing (Fujita and Spikes 2004), such as soluble $Fe^{2+}$ or $Fe^{3+}$. By *ligand exchange*, the iron ion replace the zinc in ZDDP to form a less thermally stable metal dithiophosphate, which subsequently decomposes (Piras *et al*. 2003) at lower temperatures to form iron phosphate glass in a reaction similar to that which occurs for ZDDP at higher temperatures The formation of an iron phosphate layer on the steel surface predominantly occurs at the beginning of the experiment where there is substantial steel–steel contact as no, or hardly any, protective layer has formed. This would also establish the autocatalytic reaction so that ZDDP can subsequently decompose directly (Fujita and Spikes 2005). The process can also be triggered by triboelectronic processes, such as exoelectron emission, and a subsequent negative ion reaction (Kajdas 2005).

The reaction layer rapidly develops until reaching saturation. At this point, the steel surface is

TABLE III Wear track width, friction coefficient, and reaction layer thickness

| | | Parameters | | |
|---|---|---|---|---|
| Sample | Rubbing time (min) | Average friction coefficient, μ | Wear track width (μm) | Reaction layer thickness (nm) |
| ZDDP1 | 5 | 0.086 ± 0.002 | 540.1 ± 4.4 | 13.3 ± 2.3 |
| ZDDP2 | 15 | 0.092 ± 0.001 | 503.7 ± 2.5 | 53.3 ± 1.2 |
| ZDDP3 | 30 | 0.089 ± 0.002 | 508.3 ± 2.6 | 70.8 ± 2.1 |
| ZDDP4 | 60 | 0.083 ± 0.005 | 574.3 ± 2.5 | 79.4 ± 1.2 |
| ZDDP5 | 180 | 0.098 ± 0.003 | 589.9 ± 2.0 | 72.7 ± 1.5 |

completely covered by the reaction layer, which slows the rate of reaction layer formation. The next stage involves a wearing-out of the layer, being the rate of formation lower than the rate of removal. Owing to the reaction layer thickness, primarily the iron (rich) phosphate layer is worn, and as there is no supply of iron ions anymore the new layer formed will have $Zn^{2+}$ as counter ion. ZDDPs are more thermally stable; thus, the rate of formation is smaller than the wear of the iron rich layer leading to a decrease in the layer thickness until a final stage of equilibrium, between the rate of formation and removal, is reached. At this equilibrium stage, the layer reaches a constant thickness value or limiting thickness. The reaction layer will have an iron gradient being richer in iron close to the steel surface and richer in zinc at the layer/oil interface. At this stage, primarily the zinc rich top layer will be worn during rubbing and as there are few (or none) iron ions available the new reaction layer will be formed with zinc as counter ion, leading to an equilibrium in the rates of formation and removal (Naveira-Suarez *et al.* 2010). The initial WTW measured in sample ZDDP1, after 5 min rubbing, corresponds with the Hertzian contact diameter. The continuous rubbing leads to lower WTW values that indicate how the formation of a reaction layer protects the steel surface. However, the rubbing progression leads to a later increase in the WTW, as observed in sample ZDDP4, which also stabilizes with rubbing time.

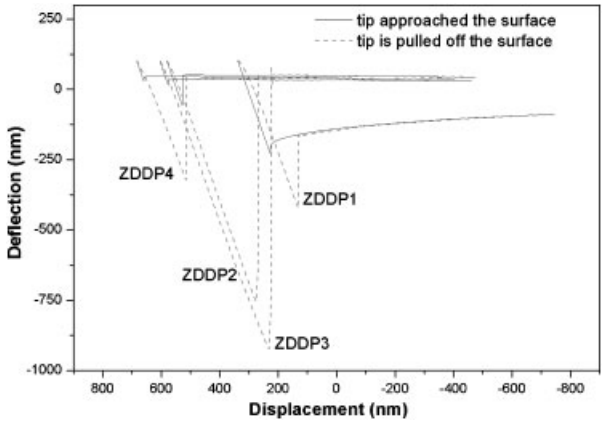


Fig 2. The deflection of the cantilever tip as a function of the distance from the wear track surface for all the investigated samples.

TABLE IV Pull-off force values

| Sample | Pull-off force (nm) | Pull-off force (nN) |
|---|---|---|
| ZDDP1 | 199.10 ± 0.23 | 19.35 |
| ZDDP2 | 697.84 ± 0.86 | 67.83 |
| ZDDP3 | 951.82 ± 0.72 | 92.51 |
| ZDDP4 | 360.28 ± 0.41 | 35.01 |

## Nanotribological Tests

In order to understand the nature of the interaction between the cantilever tip and the formed reaction layer, the deflection displacement curves were recorded. Figure 2 shows the deflection of the cantilever tip as a function of the distance from the reaction layer formed in the rubbing steel surfaces. The solid line indicates the tip approach to the surface, whereas the dashed line represents the tip being pulled away from the surface. The vertical separation between the point where the tip was touching the layer and the point where the tip was pulled away from it together with spring constant of the cantilever (0.1 nN/nm) were used to calculate the pull-off (adhesive) force (Bhushan 2005), see Table IV.

Figure 2 shows that with increasing the ZDDP-derived reaction layer thickness, the force needed to pull-off the cantilever from the surface also increases. This fact is related to high adhesion and plastic deformation, due to the presence of a soft surface layer formed by ZDDP. For sample ZDDP1, the reaction layer is thin (13.3 nm) and does not cover the surface homogenously. Short deflection displacement curve is due to contact of the cantilever with asperities from steel surface while engaging. For sample ZDDP4, after 1 h test, the additive-derived reaction layer becomes stable and harder, as suggested by the nanowear results (Table V, Figs. 4, 6, 8, and 10), as the adhesion forces are subsequently reduced.

The three-dimensional AFM images showing the topographies of the ZDDP-derived layers are illustrated in Table V (Figs. 3, 5, 7, and 9). Section graphs attached to the AFM images show the height

TABLE V AFM images showing the topographies of the investigated samples before and after nanowear indentation with section graphs of height distribution for wear volume calculation

| Before indentation | After indentation |
|---|---|
| ZDDP1–PAO+ZDDP, 300 N, 90°C, 0.25 m/s, (−)10% SRR – 5 min | ZDDP1 $V = 0.272\ \mu m^3$ |
| ZDDP2–PAO+ZDDP, 300 N, 90°C, 0.25 m/s, (−)10% SRR–15 min | ZDDP2 $V = 0.425\ \mu m^3$ |
| ZDDP3–PAO+ZDDP, 300 N, 90°C, 0.25 m/s, (−)10% SRR–30 min | ZDDP3 $V = 0.475\ \mu m^3$ |
| ZDDP4–PAO+ZDDP, 300 N, 90°C, 0.25 m/s, (−)10% SR–1 h | ZDDP4 No wear scare |

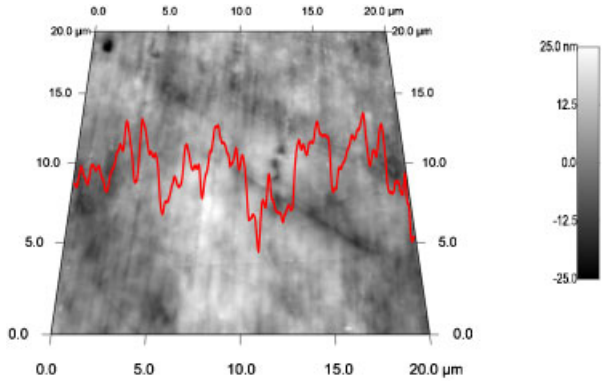


Fig 3. AFM image showing the topography of the investigated sample before nanowear indentation with section graph of height distribution. ZDDP1–PAO+ZDDP, 300 N, 90°C, 0.25 m/s, (−)10% SRR–5 min, $20 \times 20\ \mu m^2$ topography. AFM, atomic force microscopy; ZDDP, zinc dialkyl dithiophosphates; PAO, poly-α-olefin; SRR, slide-roll ratio.

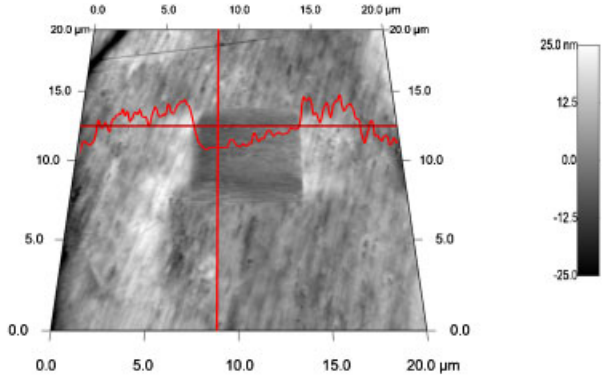


Fig 4. ZDDP1, $V = 0.272\ \mu m^3$. AFM topography image after nanowear indentation with horizontal section profile for wear volume calculation. AFM, atomic force microscopy; ZDDP, zinc dialkyl dithiophosphates.

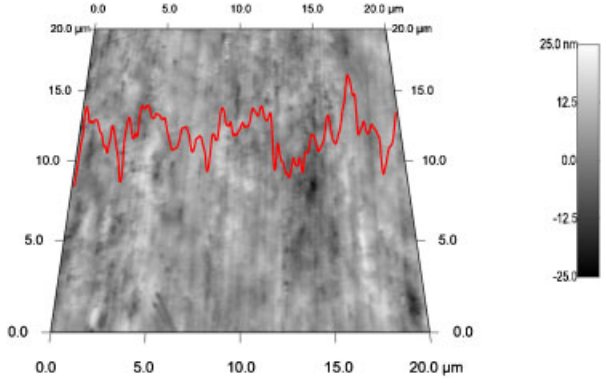


Fig 5. AFM image showing the topography of the investigated sample before nanowear indentation with section graph of height distribution. ZDDP2–PAO+ZDDP, 300 N, 90°C, 0.25 m/s, (−)10% SRR–15 min $20 \times 20\ \mu m^2$ topography. AFM, atomic force microscopy; ZDDP, zinc dialkyl dithiophosphates; PAO, poly-α-olefin; SRR, slide-roll ratio.

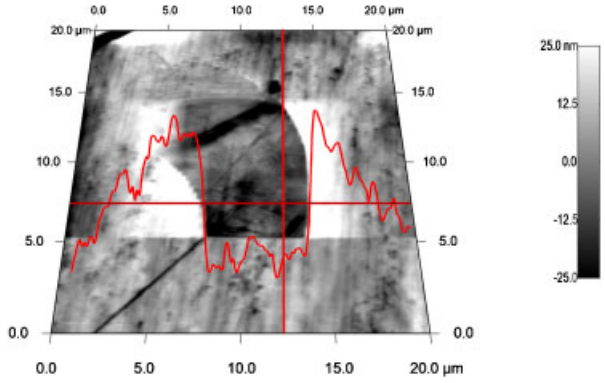


Fig 6. ZDDP2, $V = 0.425\ \mu m^3$. AFM topography image after nanowear indentation with horizontal section profile for wear volume calculation. AFM, atomic force microscopy; ZDDP, zinc dialkyl dithiophosphates.

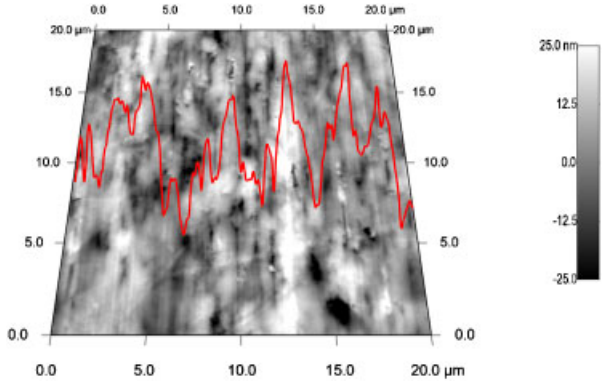


Fig 7. AFM image showing the topography of the investigated sample before nanowear indentation with section graph of height distribution. ZDDP3–PAO+ZDDP, 300 N, 90°C, 0.25 m/s, (−)10% SRR–30 min, $20 \times 20\ \mu m^2$ topography. AFM, atomic force microscopy; ZDDP, zinc dialkyl dithiophosphates; PAO, poly-α-olefin; SRR, slide-roll ratio.

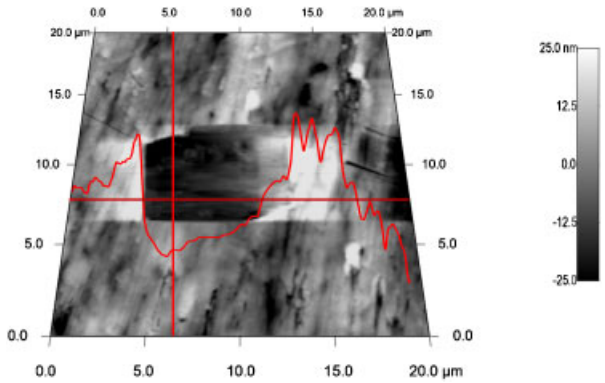


Fig 8. ZDDP3, $V = 0.475\ \mu m^3$. AFM topography image after nanowear indentation with horizontal section profile for wear volume calculation. AFM, atomic force microscopy; ZDDP, zinc dialkyl dithiophosphates.

distribution across the scan. Section graphs have the same scale as the color scale on the right side of the AFM images.

Various topographical parameters such as RMS, minimum, and maximum spot heights on the surface are given in Table VI. Parameters describing surface roughness include the autocorrelation function that compares surface heights between different points along the surface. The autocorrelation point gives a full description of roughness spacing, analogous to the height distribution for roughness height. Strictly related to the autocorrelation function is the roughness exponent $\alpha$, also called Hurst parameter. It reveals how jagged a surface with a given rms roughness and lateral correlation length is. $\alpha$ usually ranges between 0.5 (exponential decay of $C(r)$—more jagged surface) and 1 (Gaussian $C(r)$—less jagged) (Boshui *et al.* 1996). For sample ZDDP4, the Hurst parameters are close to 0.5, which is therefore the most jagged surface. This is expected because from Tables V and VI it can be observed that sample ZDDP4 appears rougher and shows more spikes compared with the other layers.

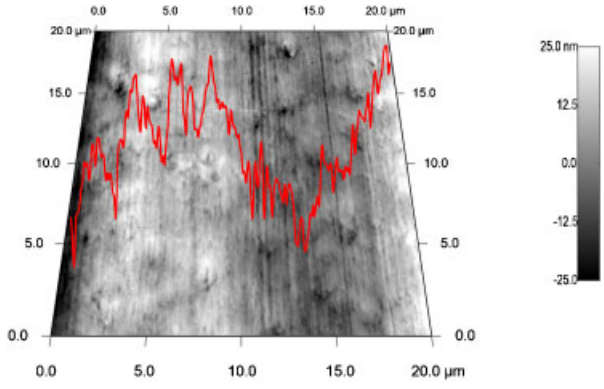


Fig 9. AFM image showing the topography of the investigated sample before nanowear indentation with section graph of height distribution. ZDDP4–PAO+ZDDP, 300 N, 90°C, 0.25 m/s, (−)10% SRR–1 h, $20 \times 20\ \mu m^2$ topography. AFM, atomic force microscopy; ZDDP, zinc dialkyl dithiophosphates; PAO, poly-α-olefin; SRR, slide-roll ratio.

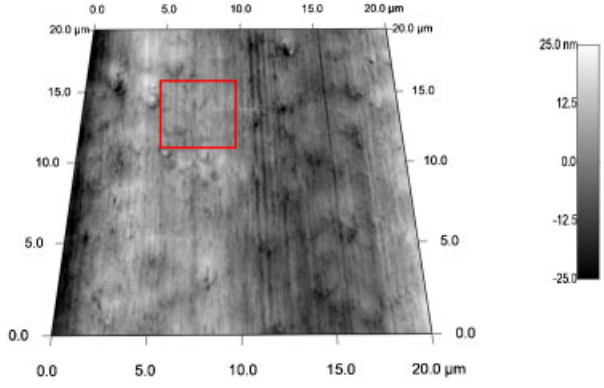


Fig 10. ZDDP4. AFM topography image after nanowear indentation with a square marking the rubbing area. AFM, atomic force microscopy; ZDDP, zinc dialkyl dithiophosphates.

The RMS values displayed in Table VI show how, in the initial stage of layer formation, a slight smoothening of the layer occurs. This process can be attributed to the gradual coverage of the first initial nucleation on asperity–asperity contacts. Sample ZDDP1, after 5 min rubbing time, presents higher roughness values than samples ZDDP2 and ZDDP3, after 15 and 30 min rubbing, respectively. The topography images show a partial coverage of the steel surface, as no surface finishing marks from the original steel surface are visible, by a very thin reaction layer from sample ZDDP1, therefore having an important influence in the roughness from the initial steel surface. When rubbing progresses, a thicker layer develops, growing from distinct reaction events on micro-asperity contacts at the steel surfaces, leading to the formation of segregated pads (Graham *et al.* 1999), as seen in the topographical images of sample ZDDP2. Further rubbing causes the pads grow and coalesce to form a complete reaction layer and a consequent smoothening of the layer, as observed for sample ZDDP3. The roughening observed when rubbing continuous is due to evolution of the reaction layer morphology, with further development of distinctive features (Aktary *et al.* 2002).

Following the procedure suggested by Beake *et al.* (2000), the friction force ($F_L$) is given by

$$F_L = 1/2(\mathrm{LF}(f) - \mathrm{LF}(r)) \quad (1)$$

where LF($f$) and LF($r$) are the signals in the forward and reverse direction of motion of the tip in LFM

TABLE VI Topographical parameters of the reaction layer formed at different rubbing times

| | | Parameters | | | |
|---|---|---|---|---|---|
| Sample | Rubbing time [min] | R.M.S roughness (nm) | Minimum height (nm) | Maximum height (nm) | Hurst parameter, α |
| ZDDP1 | 5 | 16.774 | −279.403 | 138.731 | 0.778 |
| ZDDP2 | 15 | 14.910 | −109.366 | 49.423 | 0.761 |
| ZDDP3 | 30 | 10.010 | −211.205 | 45.665 | 0.774 |
| ZDDP4 | 60 | 34.974 | −372.240 | 154.989 | 0.564 |
| ZDDP5 | 180 | 48.037 | −138.251 | 216.618 | 0.815 |

mode. This equation is based on the fact that when there is a substantial variation in the surface topography, the LFM signal contains a component due to normal force acting through the local slope. As lateral force is determined from the difference between signals reaching the left and the right halves of a four segment photo detector, the topographic contribution of the LFM image may be eliminated by subtracting signals recorded in opposite directions.

The variation of friction force as a function of load for all samples is presented in Figure 11. The highest friction is observed for sample ZDDP4 (PAO+ZDDP, 300 N, 90°C, 0.25 m/s, (−)10% SRR, 1 h). This is in good agreement with previously reported studies (Georges *et al.* 1979), due to the formation of a rougher and thicker reaction layer on the steel surface, as can be observed in the topographical images, see Tables III and V (Fig. 9). The higher friction exhibited by sample ZDDP1, corresponding to the reaction layer formed after 5 min rubbing, may be caused by the elevated asperity friction due to the low thickness of the layer. Therefore, the friction will arise mainly from the steel substrate, a less shearable material than the ZDDP-derived layers. This fact is in good agreement with pull-off force records, where sample ZDDP1 exhibits short deflection displacement curve due to contact of the cantilever with the asperities from the steel surface while engaging.

When analyzing these results one have to be aware of the limitation of the qualitative AFM analysis. To provide nanometer spatial resolution, a very sharp tip of nanometer-scale radius is used but the precise geometry of this tip is difficult to measure and can vary with use, which lead to poor repeatability from experiment to experiment. In this study, a fresh cantilever was used for every sample; however, the possible variations in the original geometry of the tips were not considered.

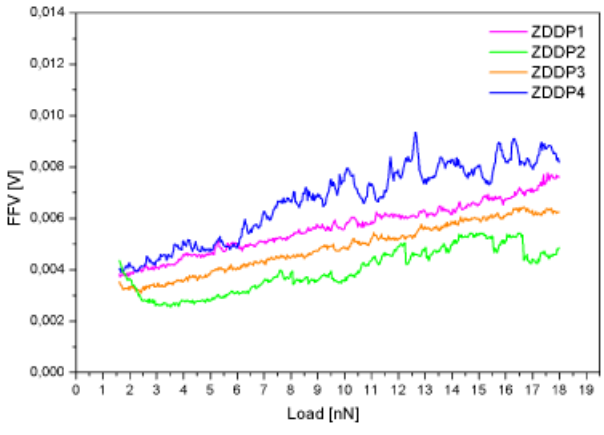


Fig 11. The variation of friction force as a function of applied load for the investigated samples.

Wear test for the ZDDP4 and ZDDP5 samples did not show any point of indentation after 40 scans of $5 \times 5\,\mu m^2$ area using a cantilever with very high spring constant at Set point 8 V (22 μN). Samples ZDDP1, ZDDP2, and ZDDP3 showed clear indentation areas as can be observed on Table V (Figs. 4, 6, and 8). The average wear volume was calculated using the average height of the horizontal and vertical profiles of the unworn area outside the indentation region (plane). Volume analysis estimates the volume occupied by the space between a surface and a plane parallel to the reference plane of the surface that intersects the maximum height of the surface. This parameter can be seen as the volume of water that the surface must hold in order to completely "submerge it." The wear volume calculations contain a measurement error due to the roughness of the layers; however, despite this fact, it can be seen from the line profiles that the indentation caused by the nanowear tests is greater that the initial roughness. Therefore, nanowear measurements enable a valid comparison among the ZDDP samples.

The wear volume calculations indicate that the ZDDP-derived layer is initially softer, undergoing a hardening process with rubbing time. The indentation reaches the steel substrate for sample ZDDP1, according to the reaction layer thickness values presented in Table III. The wear values calculated for samples ZDDP2 and ZDDP3 are very similar, showing the same tendency as presented in the macroscopic measurements, despite the existing difference in layer thickness. For both samples, the indentation created by the nanowear tests was between 20 and 30 nm in depth, and despite the uncertainty on layer base line, none of the indentations have reached the substrate. The results obtained for ZDDP4, where no indentation was observed after the nanowear test, indicate a possible hardening process parallel to the roughening process of the layer that has also been observed, with the development of pad-like features (Naveira-Suarez *et al.* 2010). Previous studies (Bhushan 2005; Aktary *et al.* 2002) have shown how those features are higher than the surroundings and present a higher hardness and elastic modulus, which is attributed to the load carrying capacity of the layer.

## Conclusions

The formation and evolution of ZDDP-derived reaction layer with rubbing time were studied using a ball-on-disk test rig, spacer layer interferometry, and AFM. The macrotribological tests results showed that initially a thin ZDDP-derived layer formed after a 5-min rubbing test (sample ZDDP1)

and then quickly develops on the rubbing surfaces with increasing rubbing time. After 15 and 30 min test (samples ZDDP2 and ZDDP3), the reaction layer thickness increased while the WTW values were reduced. That indicates how the formation of an additive-derived reaction layer protects the steel surface. The rubbing progression leads to a later increase in the WTW until a stable, rough, and hard layer develops (sample ZDDP4), reaching a ''limiting thickness'' of approximately 70 nm (sample ZDDP5).

The topography of the layer at different rubbing times, analyzed using AFM, evolves from an initial slight coverage of the surface, to the growth of a thick layer over the wear track, verifying the interferometry findings.

Sample ZDDP1 (after 5-min test) exhibits a thin reaction layer, the cantilever has alternate contact with asperities from steel surface and the layer. This results in short pull-off values when tip engage the elevated asperities and high lateral respond.

Sample ZDDP2 (15-min test) and ZDDP3 (30-min test) present a thick and soft reaction layer that covers entirely the steel surface. The cantilever interact only with the soft layer covering the surfaces resulting in long distance curves, low friction however high wear volume in nanoscale. Higher adhesive properties of the soft layer are caused by the molecular interactions between the molecules attached to the tip and the molecules on the layer.

When rubbing progresses further, the additive-derived layer experiences a constant roughening and hardening with rubbing time, as indicated by the nanowear tests, which show no indentation for the layers ZDDP4 after 1 h rubbing time. These processes may be responsible for the observed increase in friction and wear protection with rubbing time of the additive-derived reaction layers, in both the macro and the nano scale.

## Acknowledgements

The authors are grateful to the European Commission for supporting this work through their WEMESURF Training and Mobility of Researchers Network. The authors wish to thank Alexander de Vries, SKF Engineering and Research Centre Managing Director, for permission to publish this work.

## References

Aktary M, McDermott MT, McAlpine GA: Morphology and nanomechanical properties of ZDDP antiwear films as a function of tribological contact time. *Tribol Lett* **12**(3), 155–162 (2002).

American Society for Metals: *ASM Handbook*, *Vol. 18*: *Friction*, *Lubrication and Wear Technology*, ASM International, Ohio (1992).

Bancroft GM, Kasrai M, Fuller M, Yin Z: Mechanism of tribochemical film formation: stability of tribo- and thermally-generated ZDDP films. *Tribol Lett* **3**, 47–51 (1997).

Barnes AM, Bartle KD, Thibon VRA: A review of zinc dialkyldithiophosphates (ZDDPs): characterisation and role in the lubricating oil. *Tribol Int* **34**, 389–395 (2001).

Beake BD, Hassan IU, Rego CA, Ahmed W: Friction force microscopy study of diamond films modified by a glow discharge treatment. *Diamond Relat Mater* **9**(8), 1421–1429 (2000).

Bec S, Tonck A, Georges JM, Coy RC, Bell JC, *et al.*: Relationship between mechanical properties and structures of zinc dithiophosphate anti-wear films. *Proc R Soc A Math Phys Eng Sci* **455**, 4181–4203 (1999).

Bhushan B: *Nanotribology and Nanomechanics—An Introduction*, Springer, Berlin (2005).

Bird RJ, Galvin GD: The application of photoelectron spectroscopy to the study of e.p. films on lubricated surfaces. *Wear* **37**(1), 143–167 (1976).

Boshui C, Junxiu D, Guoxu C: Tribochemistry of gadolinium dialkyldithiophosphate. *Wear* **196**(1–2), 16–20 (1996).

Cann PM, Hutchinson J, Spikes HA: The development of a spacer layer imaging method (SLIM) for mapping elastohydrodynamic contacts. *Tribol Trans* **39**(4), 915–921 (1996).

Coy RC, Jones RB: Thermal degradation and EP performance of zinc dialkyldithiophosphates additives in white oil. *ASLE Trans* **24**(1), 77–90 (1981).

Donnet C: *Handbook of Surface and Interface Analysis—Methods for Problem-Solving*, Marcel Dekker, Basel (1998).

Eglin M, Rossi A, Spencer ND: X-ray photoelectron spectroscopy analysis of tribostressed samples in the presence of ZnDTP: a combinatorial approach. *Tribol Lett* **15**(3), 199–209 (2003).

Fujita H, Spikes HA: Study of zinc dialkyldithiophosphate antiwear film formation and removal processes, part I: experimental. *Tribol Trans* **48**(4), 558–566 (2005).

Fuller M, Yin Z, Kasrai M, Bancroft GM, Yamaguchi ES, *et al.*: Chemical characterization of tribochemical and thermal films generated from neutral and basic ZDDPs using X-ray absorption spectroscopy. *Tribol Int* **30**(4), 305–315 (1997).

Gellman AJ, Spencer ND: Surface chemistry in tribology. *Proc Inst Mech Eng* [*J*] **216**(6), 443–461 (2002).

Georges JM, Martin JM, Mathia T, Kapsa P, Meille G, *et al.*: Mechanism of boundary lubrication with zinc dithiophosphate. *Wear* **53**(1), 9–34 (1979).

Graham JF, McCague C, Norton PR: Topography and nanomechanical properties of tribochemical films derived from zinc dialkyl and diaryl dithiophosphates. *Tribol Lett* **6**(3), 149–157 (1999).

Heuberger R, Rossi A, Spencer ND: Pressure dependence of ZnDTP tribochemical film formation: a combinatorial approach. *Tribol Lett* **28**(2), 209–222 (2007a).

Heuberger R, Rossi A, Spencer ND: XPS study of the influence of temperature on ZnDTP tribofilm composition. *Tribol Lett* **25**(3), 185–196 (2007b).

Jianqiang H, Huanqin Z, Li W, Xianyong W, Feng J, *et al.*: Study on tribological properties and action mechanism of organic cadmium compound in lubricants. *Wear* **259**(1–6), 519–523 (2005).

Kajdas CK: Importance of the triboemission process for tribochemical reaction. *Tribol Int* **38**(3), 337–353 (2005).

Martin JM, Grossiord C, Le Mogne T, Bec S, Tonck A: The two-layer structure of Zndtp tribofilms, Part I: AES,

XPS and XANES analyses. *Tribol Int* **34**(8), 523–530 (2001).

Minfray C, Martin JM, Esnouf C, Le Mogne T, Kersting R, Hagenhoff B: A multi-technique approach of tribofilm characterisation. *Thin Solid Films* **447**, 272–277 (2004).

Minfray C, Le Mogne T, Lubrecht AA, Martin J-M: Experimental simulation of chemical reactions between ZDDP tribofilms and steel surfaces during friction processes. *Tribol Lett* **21**(1), 65–76 (2006).

Naveira-Suarez A, Zaccheddu M, Grahn M, Pasaribu R, Larsson R: Parameters affecting the functionality of additives in tribological contacts — An experimental and molecular dynamics simulation study. *Proceedings of the IV World Tribology Congress*, Kyoto, Japan, 66 (2009).

Naveira-Suarez A, Zaccheddu M, Grahn M, Pasaribu R, Larsson R: The influence of base oil polarity and slide-roll ratio on additive derived reaction layer formation. *Proceedings of the 14th Nordic Symposium in Tribology* (*NordTrib 2010*), Storforsen, Sweden (2010).

Piras FM, Rossi A, Spencer ND: Combined in situ (ATR FT-IR) and ex situ (XPS) study of the ZnDTP-iron surface interaction. *Tribol Lett* **15**(3), 181–191 (2003).

Sakamoto T, Uetz H, Föhl J: Reaction layer formation on bronze with an S-P extreme pressure additive in boundary lubrication under increasing load: I. *Wear* **105**(4), 307–321 (1985).

Sarin R, Tuli DK, Verma AS, Rai MM, Bhatnagar AK: Additive-additive interactions: search for synergistic FM-EP-AW composition. *Wear* **174**(1–2), 93–102 (1994).

Spedding H, Watkins RC: Antiwear mechanism of ZDDP's—1. *Tribol Int* **15**(1), 9–12 (1982).

Taylor L, Dratva A, Spikes HA: Friction and wear behavior of zinc dialkyldithiophosphate additive. *Tribol Trans* **43**(3), 469–479 (2000).

Taylor LJ, Spikes HA: Friction-enhancing properties of ZDDP antiwear additive: part I—friction and morphology of ZDDP reaction films. *Tribol Trans* **46**(3), 303–309 (2003).

Tomala A, Naveira-Suarez A, Gebeshuber IC, Pasaribu R: Effect of base oil polarity on micro and nanofriction behaviour of base oil+ZDDP solutions. *Tribol Mater Surf Interfaces* **3**(4), 182–188 (2009).

Torrance AA, Morgan JE, Wan GTY: An additive's influence on the pitting and wear of ball bearing steel. *Wear* **192**, 66–73 (1996).

Watkins RC, Spedding H: Antiwear mechanism of ZDDP's—2. *Tribol Int* **15**(1), 13–15 (1982).

Willermet PA, Carter RO, Schmitz PJ, Everson M, Scholl DJ, *et al.*: Formation, structure, and properties of lubricant-derived antiwear films. *Lubrication Sci* **9**(4), 325–348 (1997).

Willermet PA, Dailey DP, Carter III RO, Schmitz PJ, Zhu W: Mechanism of formation of antiwear films from zinc dialkyldithiophosphates. *Tribol Int* **28**(3), 177–187 (1995a).

Willermet PA, Dailey DP, Carter RO, Schmitz PJ, Zhu W, *et al.*: The composition of lubricant-derived surface layers formed in a lubricated cam/tappet contact II. Effects of adding overbased detergent and dispersant to a simple ZDTP solution. *Tribol Int* **28**(3), 163–175 (1995b).

Yin Z, Kasrai M, Bancroft GM, Laycock KF, Tan KH: Chemical characterization of antiwear films generated on steel by zinc dialkyl dithiophosphate using X-ray absorption spectroscopy. *Tribol Int* **26**(6), 383–388 (1993).

Yin Z, Kasrai M, Fuller M, Bancroft GM, Fyfe K, *et al.*: Application of soft x-ray absorption spectroscopy in chemical characterization of antiwear films generated by ZDDP Part II: the effect of detergents and dispersants. *Wear* **202**(2), 192–201 (1997).

Zhang J, Liu W, Xue Q, Wang Q: Investigation of the friction and wear behaviors of Cu(I) and Cu(II) dioctyldithiophosphates as additives in liquid paraffin. *Wear* **216**(1), 35–40 (1998).